INTERNATIONAL TRANSACTIONS IN OPERATIONAL RESEARCH

Intl. Trans. in Op. Res. XX (20XX) 1–20
DOI: xx.xxxx/itor.xxxxx

Beam Angle Optimization in IMRT: Are We Really Optimizing What Matters?

H. Rocha[a,b,*], J. M. Dias[a,b], T. Ventura[c], B. C. Ferreira[d,e] and M. C. Lopes[c,e]

[a]*FEUC and CeBER, Av. Dias da Silva 165, 3004–512 Coimbra, Portugal*
[b]*INESCC, Rua Silvio Lima, 3030-290 Coimbra, Portugal*
[c]*IPOC-FG, EPE, Av. Bissaya Barreto 98, 3000–075 Coimbra, Portugal*
[d]*ESS.PP, Rua Valente Perfeito 322, 4400–330 Vila Nova de Gaia, Portugal*
[e]*I3N.UA, Departamento de Fisica, Universidade de Aveiro, 3810–193 Aveiro, Portugal*
E-mail: hrocha@mat.uc.pt [H. Rocha]; joana@fe.uc.pt [J. M. Dias];
tiagoventura@ipocoimbra.min-saude.pt [T. Ventura];
bcf@ess.ipp.pt [B. C. Ferreira];
mclopes@ipocoimbra.min-saude.pt [M. C. Lopes]

Received DD MMMM YYYY; received in revised form DD MMMM YYYY; accepted DD MMMM YYYY

Abstract

Intensity-modulated radiation therapy (IMRT) is a modern radiotherapy modality that uses a multileaf collimator to enable the irradiation of the patient with non-uniform maps of radiation from a set of distinct beam irradiation directions. The aim of IMRT is to eradicate all cancerous cells by irradiating the tumor with a prescribed dose while simultaneously sparing, as much as possible, the neighboring tissues and organs. The optimal choice of beam irradiation directions – beam angle optimization (BAO) – can play an important role in IMRT treatment planning by improving organ sparing and tumor coverage, increasing the treatment plan quality. Typically, the BAO search is guided by the optimal value of the fluence map optimization (FMO) – the problem of obtaining the most appropriate radiation intensities for each beam direction. In this paper, a new score to guide the BAO search is introduced and embedded in a parallel multistart derivative-free optimization framework that is detailed for the extremely challenging continuous multi-modal BAO problem. For the set of ten clinical nasopharyngeal tumor cases considered, treatment plans obtained for optimized beam directions clearly outperform the benchmark treatment plans obtained considering equidistant beam directions typically used in clinical practice. Furthermore, treatment plans obtained considering the proposed score clearly improve the quality of the plans resulting from the use of the optimal value of the FMO problem to guide the BAO search.

Keywords: Intensity-modulated radiation therapy; Beam angle optimization; Parallel multistart; Derivative-free optimization

*Author to whom all correspondence should be addressed (e-mail: hrocha@mat.uc.pt).

1. Introduction

Cancer is a continuously increasing health problem with respect to its mortality and incidence features. Radiation therapy (RT) is used for more than half of the cancer patients, either with curative intent or simply to give important symptom relief. The aim of RT is to eradicate all cancerous cells by irradiating the tumor with a prescribed dose while simultaneously sparing, as much as possible, the neighboring tissues and organs. Intensity-modulated radiation therapy (IMRT) is a modern type of RT that uses a multileaf collimator to transform the radiation beam into a discrete set of small beamlets with different intensities (Figure 1). This discretization of the radiation beam is used for a more accurate control of the three-dimensional dose distribution. The problem of optimizing the radiation intensities is usually known as fluence map optimization (FMO), and is usually a large-scale programming problem that requires the computation of algorithms to achieve valuable solutions.

In IMRT, radiation is usually generated by a linear particle accelerator mounted on a C-arm gantry capable of rotating along a central axis. Selected radiation beams irradiate the tumor, from different directions, depositing in an additive way the total radiation dose in the tumor while aiming to spare the surrounding tissues and organs. In clinical practice, equispaced coplanar irradiation directions are typically used, i.e. beam angle directions evenly distributed on the plane of rotation of the linear accelerator's gantry. However, the choice of appropriate beam irradiation directions – beam angle optimization (BAO) – can enhance treatment plan quality (Das and Marks, 1997). Furthermore, for particular tumor sites, as for intra-cranial tumors, the use of optimized beam irradiation directions substantially improves treatment plan quality (Bangert et al., 2013). The main reason for the clinical use of equispaced beam angle ensembles is inherent to the challenge of solving the BAO problem, a non-convex problem with many local minima on a vast search space (Craft, 2007).

The problems of finding the optimal beam angle directions and the corresponding optimal radiation maps can be addressed sequentially, considering geometric features or dosimetric surrogates as quality measures of the beam angle ensembles to guide the BAO search (Bangert and Oelfke, 2010; Llacer et al., 2009). Alternatively, BAO and FMO problems can be solved simultaneously and the optimal FMO value is used as quality measure of the beam angle ensembles. The second approach is predominant in the literature as it grants reliability and optimality as beam angle directions for IMRT are often non-intuitive (Stein et al., 1997). Two different mathematical formulations for the BAO problem have been used. A combinatorial BAO formulation can be obtained by considering a discrete subset of all possible angle directions in $[0, 360]$. Many different algorithms have been used to address the combinatorial BAO problem, including gradient search (Craft, 2007), neighborhood search (Aleman et al., 2008), response surface approaches (Aleman et al., 2009), branch-and-prune (Lim and Cao, 2012), hybrid approaches (Bertsimas et al., 2013), genetic algorithms (Dias et al., 2014) or matheuristic approaches (Cabrera et al., 2018). Alternative combinatorial strategies have been proposed as the combinatorial BAO problem is an NP hard problem (Bangert et al., 2012). One of the most successful is iterative BAO that adds sequentially one beam at a time to a treatment plan, decreasing the possible number of combinations (Bangert et al., 2012; Breedveld et al., 2012). An alternative methodological approach considers all possible (continuous) angles resulting in a continuous BAO formulation. Different strategies have been used to explore the BAO continuous search space (Rocha et al., 2013a,b,c, 2016).

The use of the optimal FMO value as measure of quality of a beam angle ensemble has a major drawback: the objective functions typically used to drive the FMO problem have no clinical relevance.

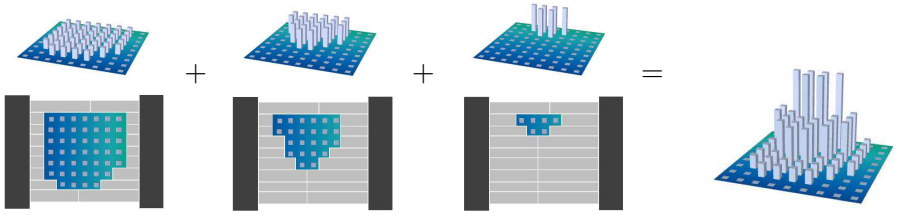

Figure 1. Illustration of a multileaf collimator (with 9 pairs of leaves) with different apertures and corresponding radiation maps whose superimposition originate an intensity map with different beamlet intensities.

The medical dose prescription for a given patient defines constraints that have to be fulfilled so that a treatment plan can be considered admissible. These constraints are related to dosimetric values. For some patients it is not possible to assure that all the constraints are indeed simultaneously fulfilled. Most FMO objective functions try to use a measure of how far the current plan is from fulfilling the medical prescription constraints, or some measure related to tumor control probabilities. These aggregated values, that are usually associated to importance weights, bounds or other predetermined parameters, have no clinical meaning whatsoever. So, FMO objective function is actually a technical tool used to guide the search procedure, but it is not used to assess the clinical quality of a treatment plan. In the clinical medical practice, the validation and selection of treatment plans explicitly considers a set of dosimetric values.

In this paper, a new score based on clinical dosimetric values weighted by its clinical importance, as described by Ventura et al. (2016), is introduced and embedded in a parallel multistart derivative-free optimization framework that explores thoroughly the BAO problem continuous search space. Preliminary tests using this score to guide a simpler BAO search lead to promising results for a single patient case (Rocha et al., 2017). Unlike previous scores proposed for BAO, this score is obtained after solving the FMO problem and thus BAO and FMO are considered simultaneously. Ten nasopharyngeal (intracranial) tumor cases already treated at the Portuguese Institute of Oncology of Coimbra (IPOC) are used to test and compare multistart BAO driven by the proposed score against multistart BAO driven by the optimal FMO value. The paper is organized as follows. A mathematical formulation of the continuous noncoplanar BAO problem is presented in the next section. In section three we describe a parallel multistart derivative-free optimization framework for the continuous noncoplanar BAO problem. Computational tests are presented in section four. In the last section we have the conclusions.

2. Noncoplanar BAO problem formulation

All possible continuous noncoplanar beam irradiation directions are considered for the mathematical formulation of the noncoplanar BAO problem. Let n be defined *a priori* by the treatment planner as the number of noncoplanar beam irradiation directions. Let the couch and the gantry angles be denoted by ϕ and θ, respectively. An unbounded mathematical formulation can be considered as angle directions -1° and 359° or angle directions 361° and 1° are equivalent. Considering an objective function (measure

or score) where the best noncoplanar beam ensemble is attained at the function's minimum, a simple mathematical formulation for the continuous noncoplanar BAO problem is:

$$\begin{aligned} \min \quad & f\Big((\theta_1,\phi_1),\ldots,(\theta_n,\phi_n)\Big) \\ s.t. \quad & \Big(\theta_1,\ldots,\theta_n,\phi_1,\ldots,\phi_n\Big) \in \mathbb{R}^{2n}. \end{aligned} \tag{1}$$

For an immobilized couch at $\phi = 0^\circ$, i.e. for coplanar BAO, the gantry will never collide with the couch. However, for noncoplanar irradiation directions, i.e. moving the couch position, collisions between couch and gantry may occur. Thus, selection of noncoplanar irradiation directions has collision restrictions. The unbounded mathematical formulation of the continuous noncoplanar BAO problem (1) can still be considered if the objective function incorporates collision restrictions in the form of a penalty. In this paper, two distinct objective functions $f\Big((\theta_1,\phi_1),\ldots,(\theta_n,\phi_n)\Big)$ used to assess the quality of a beam ensemble $(\theta_1,\phi_1),\ldots,(\theta_n,\phi_n)$ will be compared. The first one is the optimal FMO value calculated for each beam angle ensemble, embedding a penalization for beam angle candidates that allow the gantry and the couch to collide:

$$f\Big((\theta_1,\phi_1),\ldots,(\theta_n,\phi_n)\Big) = \begin{cases} +\infty & \text{if collisions occur} \\ \text{optimal FMO value} & \text{otherwise.} \end{cases}$$

This approach is the one usually found in the literature. The second, is a treatment plan's quality score calculated for each beam angle ensemble and also embedding a penalization for beam angle candidates that lead to collisions between the couch and the gantry:

$$f\Big((\theta_1,\phi_1),\ldots,(\theta_n,\phi_n)\Big) = \begin{cases} +\infty & \text{if collisions occur} \\ \text{plan's quality score} & \text{otherwise.} \end{cases}$$

Formulation of the FMO problem and description of the treatment plan's quality score are presented next.

2.1. Formulation of the FMO problem

The goal of a radiotherapy treatment plan is to deliver dose to some structures (tumors) while preventing the remaining structures to receive (too much) dose. This means that the FMO problem is inherently a multiobjective problem, since different conflicting objectives have to be simultaneously considered. The desire to explicitly consider the tradeoffs between the different conflicting objectives justify the choice of a multicriteria based FMO problem. In this paper we consider a multicriteria optimization based on the *a priori* creation of a wish-list (Breedveld et al., 2007, 2009, 2012). This methodology has proven to be able to obtain high quality treatment plans.

For the nasopharyngeal tumor clinical cases used in our tests, the wish-list constructed is displayed in Table 1. Intra-cranial tumor cases are difficult to plan given the multitude of organs in the close neighborhood of the tumor. The organs at risk (OARs) considered in the wish-list are the spinal cord,

Table 1
Wish-list for the nasopharyngeal tumor cases.

	Structure	Type	Priority	Goal	Parameters	Sufficient
Constraints	PTV_{70}	maximum		74.9 Gy (=107% of prescribed dose)		
	PTV_{59}	maximum		63.6 Gy (=107% of prescribed dose)		
	PTV_{59} shell	maximum		63.6 Gy (=107% of prescribed dose)		
	Ring PTV_{70}	maximum		59.5 Gy (=85% of prescribed dose)		
	Ring PTV_{59}	maximum		50.5 Gy (=85% of prescribed dose)		
	Spinal cord	maximum		45 Gy		
	Brainstem	maximum		54 Gy		
	Body	maximum		80 Gy		
	External Ring	maximum		45 Gy		
Objectives	PTV_{70}	LTCP	1	1	T_i = 70 Gy; α= 0.75	0.5
	PTV_{59}	LTCP	2	1	T_i = 59.4 Gy; α= 0.75	0.5
	PTV_{59} shell	LTCP	3	1	T_i = 59.4 Gy; α= 0.75	0.5
	External ring	maximum	4	42.75 Gy	–	–
	Spinal cord	maximum	5	42.75 Gy	–	–
	Brainstem	maximum	6	51.3 Gy	–	–
	Parotids	mean	7	50 Gy	–	–
	Oral cavity	mean	8	45 Gy	–	–
	Parotids	mean	9	26 Gy	–	–
	Oral cavity	mean	10	35 Gy	–	–

brainstem, parotids and oral cavity. The planning target volume (PTV), the tumor volume plus a ring that adds a safety margin, have two different dose prescription levels: a lower dose radiation (59.4Gy) was prescribed for the lymph nodes (PTV_{59}) and a higher dose radiation (70Gy) was prescribed for the tumor (PTV_{70}). Some auxiliary structures are also defined, in order to promote the fulfilling of some dosimetric constraints. Creating a margin of 10 mm from PTV_{70} to PTV_{59} originate the structure PTV_{59} shell that aims to prevent over-irradiation of the lymph nodes. Ring PTV_{70} and Ring PTV_{59} are two ring shape structures 10 mm wide surrounding PTV_{70} and PTV_{59}, respectively, aiming to improve PTV conformity and coverage. Finally, a ring 10 mm wide was created around the patient, External Ring, aiming to avoid high entrance dose values.

The wish-list is composed of nine (hard) constraints and ten hierarchical objectives. These constraints and prioritized objectives are anchored on prescribed and tolerance doses for the different structures included in the treatment planning optimization and radiation oncologist preferences. While the maximum-dose constraints have to be strictly fulfilled, the objectives are sequentially optimized following the wish-list priority order defined *a priori*. For each objective, a desired goal is defined. Objectives with higher priorities are more likely to reach the defined goal. This means that preferences of the radiation oncologist play an important role in the definition of the wish-list. Maximum-dose constraints are considered for serial organs, i.e. organs whose functionality is compromised even if only a small subunit is damaged. Spinal cord and brainstem are the serial organs included in the wish-list. Mean-dose constraints are considered for parallel organs, i.e. organs whose functionality is not compromised even if a small subunit is damaged. Parotids, the larger salivary glands, and oral cavity, that contains the remaining salivary glands, are the parallel organs included in the wish-list.

The objective considered for PTV dose optimization was the logarithmic tumor control probability

($LTCP$) (Breedveld et al., 2012),

$$LTCP = \frac{1}{N_T} \sum_{l=1}^{N_T} e^{-\alpha(D_i - T_i)},$$

where N_T corresponds to the number of voxels in the PTV, D_i corresponds to the dose in voxel i, T_i corresponds to the prescribed dose, and α corresponds to the cell sensitivity parameter. $LTCP$ penalizes doses under the prescribed value while $LTCP$ slowly tends to zero for doses D_i above the prescribed dose T_i. The ideal plan has a dose equal to T_i for each PTV voxel which corresponds to $LTCP = 1$. Tumor coverage, i.e. the percent of the PTV volume that receives at least 95% of the prescribed dose, can be enhanced for larger values of α.

A primal-dual interior-point algorithm, $2p\epsilon c$ (Breedveld et al., 2007), was used to address the *a priori* multicriteria FMO formulation based on the described wish-list. This algorithm generates automatically a unique Pareto optimal treatment plan for a fixed set of beam angle directions (Breedveld et al., 2007). The algorithm $2p\epsilon c$ has two stages. In the first stage objectives are sequentially optimized one at a time, following the hierarchy of the wish-list. Preceding the next objective, a constraint is added in order to guarantee that the outcome of the previous higher-order objective is not jeopardized when lower level priority objectives are optimized. The treatment plan reached at the end of the $2p\epsilon c$ first stage manage to comply with all the wish-list constraints as well as the goal for each objective or a higher value if the constraints avoided the desired result. Appart from tumor ($LTCP$) objectives, a full optimization for each of the remaining objectives is conducted in the second stage, following the wish-list hierarchy. For more details on interior-point algorithm $2p\epsilon c$ see Breedveld et al. (2007).

2.2. Treatment Plan's Quality Score

The quality of a treatment plan is typically assessed by resorting to a set of different clinical dose metrics. For organ sparing, the mean or maximum tolerance doses are typically the clinical dose metrics used, depending on whether the organ is parallel or serial, respectively. The clinical dose metric typically used for tumor coverage is the dose that 95% of the tumor volume receives (D_{95}). More than 95% of the dose prescribed is required. Prescribed and tolerance doses as well as the clinical dose metrics considered for the nasopharyngeal tumor cases tested are depicted in Table 2.

In this study, a score, S, incorporating the clinical dose metrics of all structures included in the treatment planning optimization procedure, is proposed as an alternative measure to guide the BAO procedure. The goal of this score is to provide a better surrogate of the quality for a given treatment plan. Analogously to the treatment plan global score proposed by Ventura et al. (2016), S is a weighted sum of each individual score assigned to every structure included in the treatment planning optimization procedure:

$$S = \sum_i w_i \times Score_i, \tag{2}$$

where w_i corresponds to the relative weight defined for structure i and $Score_i$ corresponds to the score computed for structure i. Therefore, for each structure, a relative weight has to be defined based on its

Table 2
Prescribed and tolerance doses for tumor volumes and OARs, respectively. Clinical dose metrics considered for plan's quality evaluation and respective weights.

Structure	Tolerance Dose		Prescribed	Clinical	w_i
	Mean	Max	dose	dose metrics	
$\mathbf{PTV_{70}}$	–	–	70.0 Gy	$D_{95} \geq 66.5$ Gy	0.25
$\mathbf{PTV_{59}}$	–	–	59.4 Gy	$D_{95} \geq 56.4$ Gy	0.25
Brainstem	–	54 Gy	–	$D_{max} \leq 54$ Gy	0.125
Spinal cord	–	45 Gy	–	$D_{max} \leq 45$ Gy	0.125
Left parotid	26 Gy	–	–	$D_{mean} \leq 26$ Gy	0.0625
Right parotid	26 Gy	–	–	$D_{mean} \leq 26$ Gy	0.0625
Oral cavity	45 Gy	–	–	$D_{mean} \leq 45$ Gy	0.0625
Body	–	80 Gy	–	$D_{max} \leq 80$ Gy	0.0625

clinical relevance and an individual score has to be computed considering the corresponding clinical dose metric. Similarly to the priorities of the wish-list, the radiation oncologist preferences play an important role on the definition of the relative weights that should be customized for each type of tumor in order to reflect the relative importance given by the radiation oncologist to the different planning objectives (Ventura et al., 2016). Relative weights considered for the different structures included in the treatment planning optimization procedure are depicted in the last column of Table 2. These weights correspond to the general assumption that proper irradiation of the tumor has the highest priority, followed by sparing the central nervous system organs and finally by the remaining OARs. In clinical practice, these weights should be tuned for each tumor site in order to better capture the radiation oncologist plan evaluation preferences.

Each structure's score is defined as the ratio between the clinical dose measure, i.e. the aimed dose and the corresponding planned dose, i.e. the dose obtained by the current plan. Scores for OARs and PTVs are computed as

$$Score_{OAR} = \frac{D_P}{D_C}, \tag{3}$$

$$Score_{PTV} = \frac{D_C}{D_P}, \tag{4}$$

respectively, where D_C corresponds to the clinical dose measure and D_P the dose obtained by the current plan. Thus, from (3) and (4) follows that the structure's score is equal to one if the dose for a given structure in the treatment plan is satisfying the corresponding constraint as an equality. For an improved organ sparing or target coverage a structure's score inferior to one is obtained, meaning that not only the corresponding constraint is being fulfilled, but there is also a slack in this constraint: targets are being better covered than the minimum acceptable, organs are being better spared than the minimum that would be acceptable. Overall, decreasing the S value corresponds to an improvement of the treatment plan quality.

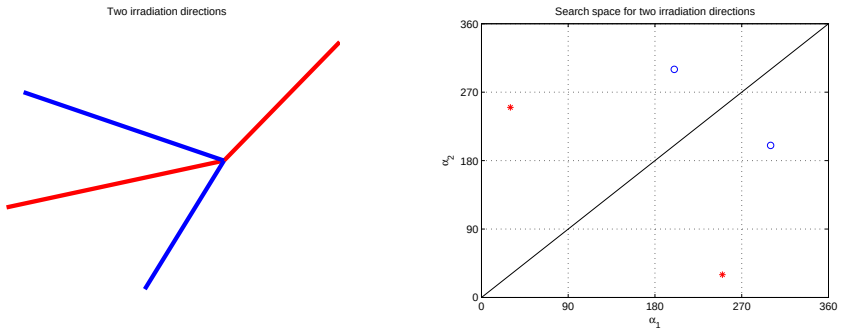

(a) (b)

Figure 2. Two pairs of coplanar orientations – 2(a). Corresponding four points in the search space $[0, 360]^2$. – 2(b).

3. Parallel multistart derivative-free optimization framework

3.1. On the continuous BAO search space

Multistart methods typically select randomly the starting points incorporating strategies to sample the entire search space. For the BAO problem, the starting points (ensembles or solutions) of a multistart procedure should be "well" spread in the entire search space $[0, 360]^n$. Due to characteristics inherent to the BAO continuous search space, a tailored selection of the starting beam angle ensembles is advised. An important characteristic of a beam angle ensemble is the fact that the beam angle's order is not important. This feature must be acknowledged in the continuous optimization of the BAO search space particularly for a parallel multistart approach.

To illustrate the interest of the irrelevance of the irradiation directions order during BAO, let us consider $n = 2$. A solution is an ordered pair $(\alpha_1, \alpha_2) \in [0, 360]^2$. However, the ordered pair $(\alpha_2, \alpha_1) \in [0, 360]^2$ is the same solution for the BAO problem. Figure 2 illustrates this symmetry, where beam directions 30° and 250°, displayed in red in Figure 2(a), have two solutions that are symmetric in the search space $[0, 360]^2$, displayed in Figure 2(b), and beam directions 200° and 300°, displayed in blue in Figure 2(a), have two solutions that are symmetric in the search space $[0, 360]^2$, displayed in Figure 2(b).

The symmetry of the solutions illustrated for two-beam ensembles in Figure 2(b) imply that, for a multistart approach, initial points placed in opposite regions of the diagonal line, lead to the exploration of the same solutions! Problems with symmetry properties are addressed in the literature using different strategies. Here, the solution is quite simple and allows the exploration of a significantly smaller proportion of the search space. If we sort all the iterates at each iteration of the BAO process, for the two-beam directions case, we assure that only one of the regions divided by the diagonal line is explored. Such strategy imply that only half of the entire search space is explored. Generically, for n-beam angle ensembles, by sorting the solution's directions, only $\frac{1}{2^n}$ of the entire search space is explored. Thus, for the five-, seven- or nine-beam ensembles BAO problem, the proportion of the entire search space explored is only 3.13% of $[0, 360]^5$, 0.78% of $[0, 360]^7$ and 0.19% of $[0, 360]^9$, respectively.

Table 3
Possible (sorted) distributions of two beam directions by the four quadrants.

α_1	α_2
1st Q	1st Q
1st Q	2nd Q
1st Q	3rd Q
1st Q	4th Q
2nd Q	2nd Q
2nd Q	3rd Q
2nd Q	4th Q
3rd Q	3rd Q
3rd Q	4th Q
4th Q	4th Q

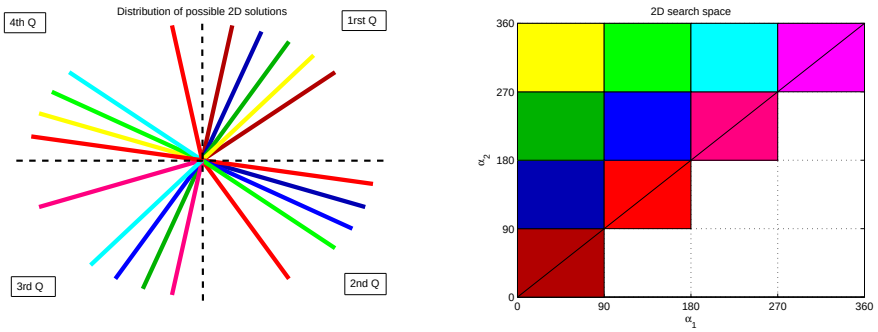

(a) (b)

Figure 3. Two beam directions possibilities for the four quadrants – 3(a). Corresponding squares in the search space $[0, 360]^2$ – 3(b).

3.2. On the sampling of the initial ensembles

The selection of the starting (sorted) beam ensembles must acknowledge the peculiarities of a reduced search space. Moreover, we must guarantee that the initial beam ensembles cover well all the reduced search space. The strategy we adopted divide the beam angle directions by quadrants and consider as starting points all the possible distributions of beam angle directions by quadrants. Let us consider again $n = 2$ for illustration purposes. In Table 3 we have all the ten different possible (sorted) distributions of two beam directions by the four quadrants. In Figure 3 examples of these ten distributions are displayed. Figure 3(a) displays examples of two beam directions for the ten cases of Table 3 while the corresponding regions (painted squares) of the reduced search space are presented in Figure 3(b). A fairly good distribution of starting points, that belong to the reduced search space and covers well that reduced search space, would place a starting point in every square. E.g., for $n = 2$ we would consider ten starting points, one for each of the ten out of twenty squares belonging to the reduced search space.

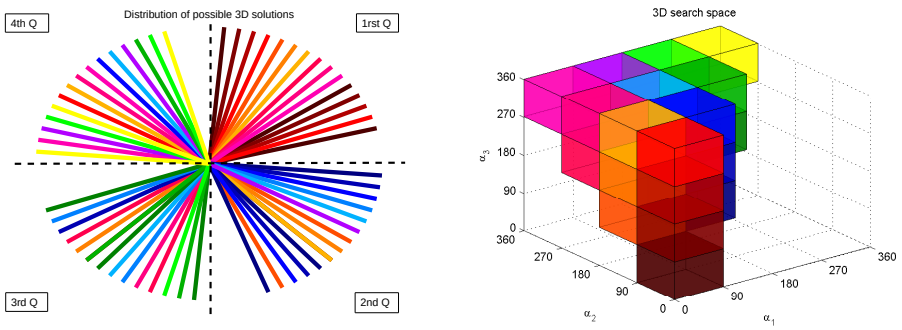

(a) (b)

Figure 4. Three beam directions possibilities for the four quadrants – 4(a) and the corresponding cubes in the search space $[0, 360]^3$ – 4(b).

In Figure 4, all the different possible distributions (20) of three beam angle directions by the four quadrants are illustrated. Figure 4(a) displays examples of three beam directions for the 20 possible cases while the corresponding regions (painted cubes) belonging to the reduced search space are presented in Figure 3(b). For $n = 3$, assigning an initial point for every cube belonging to the reduced search space, corresponds to consider 20 initial points for 20 out of 60 cubes in the search space. It is worth to highlight that the search space is reduced to half for $n = 2$ while for $n = 3$ the reduction is done by a factor of 2^2, i.e. reduced search space corresponds to 25% of the full search space. Despite a larger reduction of the search space occur for higher dimensions, the number (and dimension) of different regions belonging to the reduced search space increases. E.g., for $n = 2$ there are only ten squares while for $n = 3$ there are twenty cubes.

Generically, for $n-$beam angle ensembles, the number of (hyper)cubes of the full search space is 4^n while the reduced search space has a number of (hyper)cubes that corresponds to the combination with repetition of $\binom{n+4-1}{4} = \frac{(n+4-1)!}{4!(n-1)!}$. Thus, when considering five-, seven- or nine- beam angle ensembles, the full search space has 1024, 16384 and 262144 hypercubes compared to 56, 120 and 220 of the reduced search space, respectively.

3.3. Regions of attraction

Multistart is a two phase method. These phases are usually designated as global and local phases (Mart et al., 2013). In the global phase, the objective function is evaluated for all the initial points selected. Then, typically, search procedures are used in order to locally explore the regions around the starting points. One of the drawbacks of multistart strategies is that each local minimum can be found by distinct local procedures wasting computational time. In a broader sense, when computed in parallel, distinct local procedures may end up inspecting the same region at the same time. Clustering methods is a common strategy used to prevent different local searches to explore the same regions (Voglis and Lagaris, 2009). Regions of attraction of local minima is an alternative strategy widely used. Let $\mathcal{L}$ designate a

local search routine for the continuous BAO problem. The region of attraction of a local minimum, $\mathbf{x}^*$, can be defined as

$$A = \{\mathbf{x} \in [0, 360]^n : \mathcal{L}(\mathbf{x}) = \mathbf{x}^*\}.$$

Therefore, A corresponds to the points in $[0, 360]^n$ that would lead to the same result $\mathbf{x}^*$ by means of the local search routine $\mathcal{L}(\mathbf{x})$. A simple strategy to prevent overlap of distinct local procedures is to allow a single "active" local search routine for each region of attraction. However, in practice, it is very difficult to define a local minimum region of attraction. A common approach is to define a local minimum region of attraction as the set of points within a given radius R_A from the local minimum $\mathbf{x}^*$ (Rinnooy Kan and Timmer, 1987):

$$A = \{\mathbf{x} \in [0, 360]^n : \|\mathbf{x} - \mathbf{x}^*\| < R_A\}. \tag{5}$$

For a multistart routine computed sequentially, the regions of attraction of the local minimum sequentially found can de defined one at a time, and it is possible to determine if subsequent iterates belong to any of the previously defined regions of attraction. However, for multistart routine computed in parallel a different strategy is required as different local minima are computed simultaneously. For the parallel multistart BAO procedure, the regions of attraction are defined to be the hypercubes of the reduced search space, corresponding for $n = 2$ and $n = 3$ to the painted squares and painted cubes in Figures 3(b) and 4(b), respectively. Thus, a generalization of the region of attraction (5) is done by considering the infinity norm and the set of points within a given radius from the centroid of a given hypercube:

$$A_{BAO} = \{\mathbf{x} \in [0, 360]^n : \|\mathbf{x} - M\|_\infty < R_A\}. \tag{6}$$

3.4. Local search procedure

The non-convex nature of the BAO problem advises the selection of a local search procedure that makes no use of derivatives. In previous works, we used derivative-free algorithms to locally improve solutions computed sequentially. Pattern search methods (PSM) were selected for the resolution of the continuous BAO problem as they are able to avoid local entrapment and require a small number of function (FMO) evaluations to converge (Rocha et al., 2013a,b,c). Each iteration of PSM has two steps with different purposes. In the first step, named search step, a global search using any strategy is performed attempting to improve the outcome of the current best iterate. If the first step fails, i.e. if the search step is empty or the procedure used was not able to improve the outcome of the current best iterate, the second step, named poll step, locally explore the region around the current best iterate following the directions of positive bases. A positive basis is a set of nonzero directions (vectors) that positively span the entire search space while no subset does. The main reason for using positive bases for optimization purposes is that at least one of its vectors (directions) can provide an improvement on the objective function value unless the current iterate is a stationary point. An example of a positive basis is the set of $2n$ vectors $[I \ -I]$ where $I = [e_1 \dots e_n]$ corresponds to the identity matrix. In terms of BAO, following each direction of this positive basis corresponds to the rotation of each beam direction clockwise and counter-clockwise for a certain amount (step size) at each iteration.

The local search procedure we will use considers a pattern search method where no trial points are attempted in the search step, as global search effort is allocated to the multistart strategy, and the positive

basis considered in the poll step is $[I \ -I]$. This local search procedure corresponds to the coordinate search method. Algorithm 1 displays the parallel coordinate search algorithm used for local search.

Algorithm 1 Parallel coordinate search algorithm

Initialization:

- Set $k \leftarrow 0$;
- Choose $\mathbf{x}^0 \in \mathbb{R}^n$, $\alpha_0 > 0$ and α_{min};

Iteration:

1. Compute in parallel $f(\mathbf{x}), \forall \mathbf{x} \in \mathcal{N}(\mathbf{x}^k) = \{\mathbf{x}^k \pm \alpha_k e_i, i = 1, \ldots, n\}$.
2. If $\min_{\mathcal{N}(\mathbf{x}^k)} f(\mathbf{x}) < f(\mathbf{x}^k)$ then
   $\mathbf{x}^{k+1} \leftarrow \text{argmin}_{\mathcal{N}(\mathbf{x}^k)} \text{f}(\mathbf{x})$;
   $\alpha_{k+1} \leftarrow \alpha_k$;
   Else
   $\mathbf{x}^{k+1} \leftarrow \mathbf{x}^k$;
   $\alpha_{k+1} \leftarrow \frac{\alpha_k}{2}$;
3. If $\alpha_{k+1} \geq \alpha_{min}$ go to first step and set $k \leftarrow k + 1$.

3.5. Parallel multistart coordinate search algorithm for BAO

The strategy sketched here is tailored for the noncoplanar BAO problem. Starting points, $\mathbf{x}_i^0 \in [0, 360]^n, i = 1, \ldots, N$, with $N = \frac{(n+4-1)!}{4!(n-1)!}$, are placed in each of the hypercubes illustrated in Figures 3(b) and 4(b) for $n = 2$ and $n = 3$, respectively. For each of these initial points, the objective function value is calculated. The best solutions and corresponding objective function values found so far for each region (hypercube) are assigned to these initial points and corresponding function values: $\mathbf{x}_i^* = \mathbf{x}_i^0, i = 1, \ldots, N$; $f_i^* = f(\mathbf{x}_i^0), i = 1, \ldots, N$.

In the first iteration, a local search is performed in parallel around each starting solution on every region of attraction (hypercube) i. The iterate x_i^1, outcome of the local search around x_i^0, may or may not belong to the same region of attraction i. When iterate x_i^1 belongs to a region of attraction $j \neq i$, two different local search procedures may coexist in the same region of attraction. In order to prevent the overlap of local search procedures, only the local search yielding the iterate with lowest function value remain active. Thus, after the first iteration, some regions will have active local searches while other will not. Information of the regions that have active local searches is stored using a boolean vector, $\mathbf{Active}_{N\times 1}$, that is updated at the end of each iteration.

In a following iteration, k, the outcome of an active local search for a region of attraction i is one of the following:

- If $\mathbf{x}_i^k$ is in region i,
  — If $f(\mathbf{x}_i^k) < f(\mathbf{x}_i^*)$, i.e. if the local search is successful, the best point for region i is defined as the current iterate and the best objective function value is updated accordingly.

— If $f(\mathbf{x}_i^k) \geq f(\mathbf{x}_i^*)$ the step size is decreased. When the step size becomes inferior to lowest threshold defined (α_{min}), the local search is halted ($\mathbf{Active}_i$ is set to 0).

- If $\mathbf{x}_i^k$ is in region $j \neq i$,
  — If there are no active local searches in region j,
    * If $f(\mathbf{x}_i^k) < f(\mathbf{x}_j^*)$, i.e. if the best function value of region j is improved, then values of best iterate, best function and step size of region j are updated. Local search becomes active in region j ($\mathbf{Active}_j$ is set to 1) and inactive in region i ($\mathbf{Active}_i$ is set to 0).
    * If $f(\mathbf{x}_i^k) \geq f(\mathbf{x}_j^*)$ then local search coming from region i ends ($\mathbf{Active}_i$ is set to 0).
  — If there is an active local search in region j,
    * If $f(\mathbf{x}_i^k) < f(\mathbf{x}_j^*)$ then values of best iterate, best function and step size of region j are updated. Local search of region j ends but region j remains active ($\mathbf{Active}_j$ continues to be 1) while region i becomes inactive ($\mathbf{Active}_i$ is set to 0).
    * If $f(\mathbf{x}_i^k) \geq f(\mathbf{x}_j^*)$ then local search coming from region i ends. Region i becomes inactive ($\mathbf{Active}_i$ is set to 0).

Algorithm 2 displays the parallel multistart coordinate search algorithm.

4. Computational results

An 8-core Dell Precision T5600 with Intel Xeon processador 64GB 1600MHz was used to perform the computational tests. Erasmus-icycle, a MATLAB optimization suite developed in Rotterdam (Breedveld et al., 2007, 2009, 2012), was used to embed our parallel BAO procedure, as well as to import DICOM images, optimize dose distributions and compute and visualize dose. Erasmus-icycle optimizer, $2p\epsilon c$, was used to compute the optimal FMO values for a given beam angle ensemble.

The tailored coordinate search algorithm considered $\alpha_0 = 2^5 = 32$ as initial step size and define as stopping criteria a step size inferior to one. By choosing a power of two for initial step size and one for minimum step size, all beam angle directions considered will be integer since the step size is divided by two in case of an unsuccessful local search.

Ten nasopharyngeal (intra-cranial) tumor cases already treated at IPOC were used to test and compare BAO driven by the proposed score against BAO driven by the optimal FMO value. When IMRT (static or dynamic mode) is used, nasopharyngeal tumor cases are typically treated with five to nine coplanar equispaced beam angle directions. The parallel multistart BAO framework guided by score S and the optimal FMO value, obtained seven-beam noncoplanar treatment plans, denoted BAO_s and BAO_f, respectively. BAO_s and BAO_f plans were benchmarked against seven-beam equispaced coplanar plans, denoted *Equi*. Erasmus-iCycle was used to compute and compare all treatment plans.

Table 4 displays the values of the two measures considered for quality assessment of a beam ensemble, the optimal FMO value and S, for each of the ten patients and for each of the treatment plans, *Equi*, BAO_f and BAO_s. As expected, BAO_f treatment plans obtained the best optimal FMO value with an average improvement with respect to *Equi* treatment plans of 7.8% compared to an average improvement of 3.1% obtained by BAO_s treatment plans. On the other hand, BAO_s obtained the best S value with an average improvement with respect to *Equi* treatment plans of 7.6% compared to an average improvement of 3.6% obtained by BAO_f treatment plans.

Algorithm 2 Parallel multistart coordinate search algorithm

Initialization:

- Set $k \leftarrow 0$;
- Choose $\mathbf{x}_i^0 \in [0, 360]^n, i = 1, \ldots, N$;
- Compute $f(\mathbf{x}_i^0), i = 1, \ldots, N$ in parallel;
- Set $\mathbf{x}_i^* \leftarrow \mathbf{x}_i^0, i = 1, \ldots, N$ and $f_i^* \leftarrow f(\mathbf{x}_i^0), i = 1, \ldots, N$;
- Set $\mathbf{Active}_i \leftarrow 1, i = 1, \ldots, N$;
- Choose $\alpha_i^0 > 0, i = 1, \ldots, N$ and α_{min};

Iteration:

1. Use Algorithm 1 to locally explore, in parallel, the regions of attraction with active local search;
2. For regions of attraction i with active local search do
   If $f(\mathbf{x}_i^k) < f(\mathbf{x}_i^*)$ then
      If $\mathbf{x}_i^k$ is in region i then
         $\mathbf{x}_i^* \leftarrow \mathbf{x}_i^k$;
         $f_i^* \leftarrow f(\mathbf{x}_i^k)$;
      Else
         $\mathbf{Active}_i \leftarrow 0$;
         Determine region $j \neq i$ where $\mathbf{x}_i^k$ is;
         If $f(\mathbf{x}_i^k) < f(\mathbf{x}_j^*)$ then
            $\mathbf{x}_j^* \leftarrow \mathbf{x}_i^k$;
            $f_j^* \leftarrow f(\mathbf{x}_i^k)$;
            $\mathbf{Active}_j \leftarrow 1$;
   Else
      $\alpha_i^{k+1} \leftarrow \frac{\alpha_i^k}{2}$;
      If $\alpha_i^{k+1} < \alpha_{min}$ then
         $\mathbf{Active}_i \leftarrow 0$;
3. If there exists active regions go to first step and set $k \leftarrow k + 1$.

Despite the improvements both in terms of optimal FMO value and S, both measures are simply surrogates of the treatment plan's quality. As referred previously, clinical dose metrics are typically used to assess and compare the quality of treatment plans. These clinical dose metrics, embedded in the calculation of S, are compared in Figures 5 and 6. It is possible to acknowledge by simple inspection that BAO_s clearly outperforms both BAO_f and *Equi* treatment plans. For similar coverage of the tumor volume (Figure 5), an enhanced organ sparing is clearly obtained by BAO_s treatment plans (Figure 6).

It is straightforward to compare the three treatment plans for a given patient using the graphical analysis proposed in SPIDERplan (Ventura et al., 2016). For illustration, customized radar plots for the second patient containing all the structures included in the treatment planning optimization are displayed in Figure 7. The circular area of the radar plot is divided into sections with angles proportional to the relative weight assigned to the different structures considered. The score of each structure is represented by a point on the corresponding bisector's section matching the distance from the radar's center. The inner cir-

Table 4
Results of the beam angle optimization processes.

	Equi		BAO_f				BAO_s			
Case	FMO	S	FMO	%	S	%	FMO	%	S	%
1	771,87	0,99	709,8	8,04	0,96	3,03	750,85	2,72	0,93	6,06
2	678,37	0,93	617,19	9,02	0,9	3,23	642,78	5,25	0,85	8,60
3	734,11	0,99	665,48	9,35	0,94	5,05	721,5	1,72	0,92	7,07
4	646,62	0,97	598,28	7,48	0,96	1,03	630,78	2,45	0,91	6,19
5	694,59	0,98	655,95	5,56	0,92	6,12	677,87	2,41	0,89	9,18
6	772,28	0,99	713,47	7,62	0,95	4,04	758,03	1,85	0,91	8,08
7	566,9	0,94	511,02	9,86	0,9	4,26	548,21	3,30	0,88	6,38
8	603,9	0,97	564,38	6,54	0,94	3,09	591,36	2,08	0,91	6,19
9	820,95	0,96	761,74	7,21	0,92	4,17	774,69	5,63	0,89	7,29
10	791,97	0,98	730,29	7,79	0,96	2,04	766,14	3,26	0,91	7,14

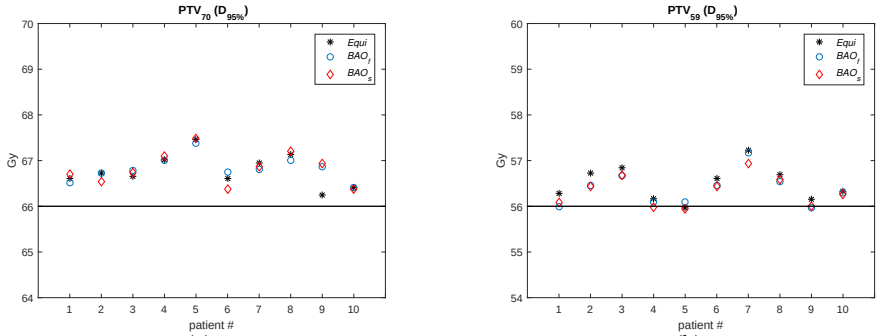

(a) (b)

Figure 5. Comparison of PTV coverage metrics obtained by *Equi*, BAO_f and BAO_s treatment plans. The horizontal lines displayed represent D_{95}.

cle in the radar plot has a radius equal to one corresponding to the case where the planned dose matches the clinical dose measure defined. Optimal scores will converge to the radar plot center while increasing deviations from prescribed/tolerance doses will converge to the outer circle with radius equal to two. The overall quality of the treatment plan is represented by the polygon connecting all the structure's scores. The inner treatment plan, corresponding to BAO_s treatment plan, is easily identified as the best treatment plan.

In clinical practice, results are also typically judged by their cumulative dose-volume histogram

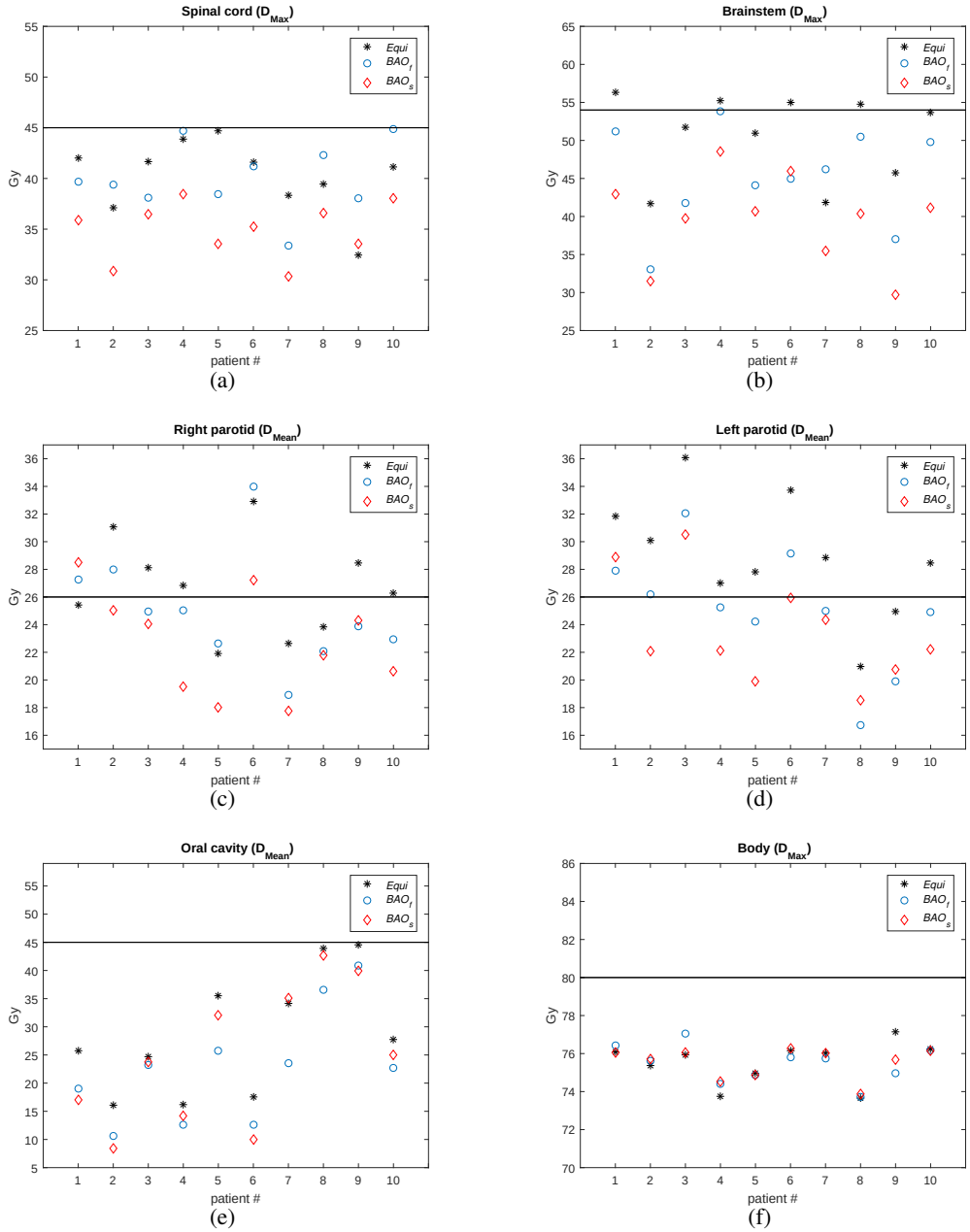

Figure 6. Comparison of organ sparing metrics obtained by *Equi*, BAO_f and BAO_s treatment plans. The horizontal lines displayed represent the tolerance (mean or maximum) dose for each structure.

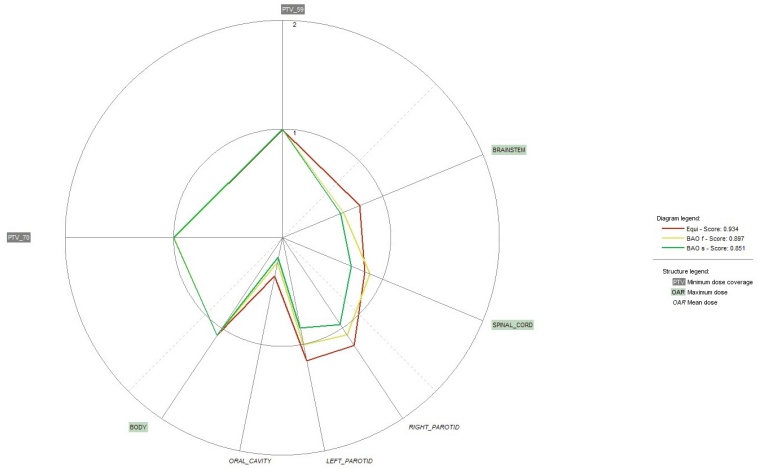

Figure 7. Radar plots comparing the results obtained by *Equi*, BAO_f and BAO_s for the second patient case.

(DVH). DVH results for the second patient are displayed in Figure 8. The DVH curves also show that for similar coverage of the tumor volumes, a clearly better sparing of the different organ's at risk is obtained by BAO_s treatment plan.

5. Conclusions

The optimal choice of beam angle directions is a very challenging optimization problem yet to be solved satisfactorily. Typically, the optimal FMO value is used as the measure of quality of a beam angle ensemble to guide the BAO search. However, the functions used for the different mathematical formulations of the FMO problem have no clinical meaning. Thus, obtaining a treatment plan with an improved optimal FMO value is not sufficient to assure that the corresponding treatment plan is preferred by the radiation oncologist. Typically, treatment plan comparison/selection rely on a set of clinical dose metrics whose relative importance depends on the tumor type and the radiation oncologist' preferences. Assuming that it is possible to define *a priori* the radiation oncologist' preferences, i.e. the relative importance of the clinical dose metrics of the different structures considered, it is possible to define a score that objectively quantifies the analysis made qualitatively by the radiation oncologist. In this paper, a new score S based on clinical dose measures weighted by relative importance was described and embedded in a multistart BAO procedure.

A parallel multistart derivative-free optimization framework was detailed and used to compare two different surrogate measures of the treatment plan's quality. This multistart derivative-free framework proved to be a competitive approach to address the noncoplanar BAO formulated as a continuous optimization problem. A global search scheme for sampling the reduced continuous BAO search space is combined with a procedure that locally improves the sampled ensembles. This scheme to disseminate starting solutions on the reduced continuous BAO search space proved to be an excellent alternative to

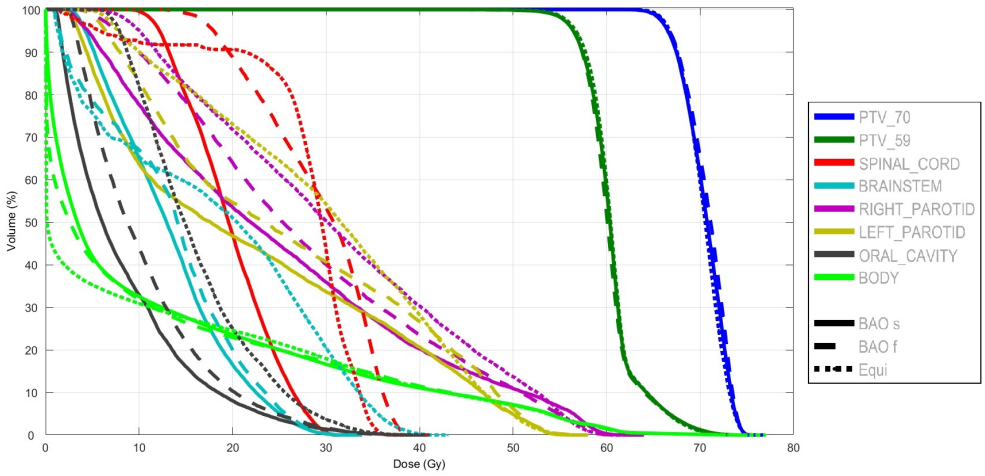

Figure 8. Cumulative dose volume histogram comparing the results obtained by *Equi*, BAO_f and BAO_s for the second patient case.

random strategies. Furthermore, it requires a fairly small number of starting solutions in order to assure a proper coverage of the entire reduced continuous BAO search space. Despite the importance of the global strategy sketched, particularly for a search space with a peculiar shape due to symmetry properties, the choice of a derivative-free method for locally improving the solutions is important to avoid local entrapment.

The multistart BAO framework guided by the two different measures manage to obtain improvements in terms of these measures. As expected, the measure that guide the search is the one with larger improvement. These improvements translate in different magnitudes of improvement of the typically used clinical dose metrics for assessing the quality of a treatment plan. For similar target coverage, an improved sparing of the OARs is clearly demonstrated by BAO_s treatment plans. For example, BAO_s plans showed an average decrease of $11,1$ Gy $(21,9\%)$ and $5,3$ Gy $(13,3\%)$ on the maximum dose of brainstem and spinal cord, respectively, and $4,1$ Gy $(15,2\%)$ and $5,4$ Gy $(18,8\%)$ on the mean dose of right and left parotids, respectively, compared to *Equi* treatment plans. More modest improvements were obtained by BAO_f plans with an average decrease of $5,5$ Gy $(10,7\%)$ and $0,2$ Gy $(0,5\%)$ on the maximum dose of brainstem and spinal cord, respectively, and $1,8$ Gy $(6,7\%)$ and $3,8$ Gy $(13,3\%)$ on the mean dose of right and left parotids, respectively, compared to *Equi* treatment plans. While improvements in brainstem and spinal cord dose metrics by BAO_s plans are impressive and important for possible cases of re-irradiation, improvements obtained in parotids are important as well. Over-irradiation of salivary glands can lead to xerostomia, decreasing the patient's quality of life. Therefore, an improved sparing of the salivary glands is important to minimize the risk of this complication, common for nasopharyngeal tumor cases.

Future work will include the integration of a larger number of structures in a score S and the clinical validation of the structure's weights. Further tests to acknowledge the advantage of this score on driving a BAO procedure should be carried on. Furthermore, one of the disadvantages of a BAO procedure guided

by the the optimal FMO value is that the beam angle ensemble found is jeopardized if a different fluence optimizer is used. It will be important to test if the BAO procedure guided by S is less dependent on the fluence optimizer, i.e. if the optimal beam ensemble found using a given treatment planning system shows the same benefits when used in a different treatment planning system.

Acknowledgements

This work has been supported by the Fundação para a Ciência e a Tecnologia (FCT) under project grant UID/MULTI/00308/2013. The authors would like to show gratitude to Ben Heijmen and Sebastiaan Breedveld for giving permission and helping them to install Erasmus-iCycle.

References

Aleman, D., Kumar, A., Ahuja, R., Romeijn, H., Dempsey, J., 2008. Neighborhood search approaches to beam orientation optimization in intensity modulated radiation therapy treatment planning. *J. Global Optim.* 42, 587–607.

Aleman, D., Romeijn, H., Dempsey, J., 2009. A response surface approach to beam orientation optimization in intensity modulated radiation therapy treatment planning. *INFORMS J. Computing: Comput.* 21, 62–76.

Bangert, M., Oelfke, U., 2010. Spherical cluster analysis for beam angle optimization in intensity-modulated radiation therapy treatment planning. *Phys. Med. Biol.* 55, 6023–6037.

Bangert, M., Ziegenhein, P., Oelfke, U., 2012. Characterizing the combinatorial beam angle selection problem. *Phys. Med. Biol.* 57, 6707–6723.

Bangert, M., Ziegenhein, P., Oelfke, U., 2013. Comparison of beam angle selection strategies for intracranial imrt. *Med. Phys.* 40, 011716.

Bertsimas, D., Cacchiani, V., Craft, D., Nohadani, O., 2013. A hybrid approach to beam angle optimization in intensity-modulated radiation therapy. *Comput. Oper. Res.* 40, 2187–2197.

Breedveld, S., Storchi, P., Heijmen, B., 2009. The equivalence of multicriteria methods for radiotherapy plan optimization. *Phys. Med. Biol.* 54, 7199–7209.

Breedveld, S., Storchi, P., Keijzer, M., Heemink, B. A.W.and Heijmen, 2007. A novel approach to multi-criteria inverse planning for imrt. *Phys. Med. Biol.* 52, 6339–6353.

Breedveld, S., Storchi, P., Voet, P., Heijmen, B., 2012. icycle: integrated, multicriterial beam angle, and profile optimization for generation of coplanar and noncoplanar imrt plans. *Med. Phys.* 39, 951–963.

Cabrera, G., Ehrgott, M., Andrew J. Mason, A.J., Raith, A., 2018. A matheuristic approach to solve the multiobjective beam angle optimization problem in intensity-modulated radiation therapy. *Intl. Trans. Op. Res.* 25, 243–268.

Craft, D., 2007. Local beam angle optimization with linear programming and gradient search. *Phys. Med. Biol.* 52, 127–135.

Das, S., Marks, L., 1997. Selection of coplanar or non coplanar beams using three-dimensional optimization based on maximum beam separation and minimized nontarget irradiation. *Int. J. Radiat. Oncol. Biol. Phys.* 38, 643–655.

Dias, J., Rocha, H., Ferreira, B., Lopes, M., 2014. A genetic algorithm with neural network fitness function evaluation for imrt beam angle optimization. *Cent. Eur. J. Oper. Res.* 22, 431–455.

Lim, G., Cao, W., 2012. A two-phase method for selecting imrt treatment beam angles: Branch-and-prune and local neighborhood search. *Eur. J. Oper. Res.* 217, 609–618.

Llacer, J., Li, S., Agazaryan, N., Promberger, C., Solberg, T., 2009. Noncoplanar automatic beam orientation selection in cranial imrt: a practical methodology. *Phys. Med. Biol.* 54, 1337–1368.

Mart, R., Resende, M., Ribeiro, C., 2013. multistart methods for combinatorial optimization. *Eur. J. Oper. Res.* 226, 1–8.

Monz, M., Kufer, K., Bortfeld, T., Thieke, C., 2008. Pareto navigationalgorithmic foundation of interactive multi-criteria imrt planning. *Phys. Med. Biol.* 53, 985–998.

Rinnooy Kan, A., Timmer, G., 1987. Stochastic global optimization problems part ii: Multi level methods. *Mathematical Programming* 39, 57–78.

Rocha, H., J., D., Ferreira, B., Lopes, M., 2013a. Beam angle optimization for intensity-modulated radiation therapy using a guided pattern search method. *Phys. Med. Biol.* 58, 2939–53.

Rocha, H., J., D., Ferreira, B., Lopes, M., 2013b. Pattern search methods framework for beam angle optimization in radiotherapy design. *Appl. Math. Comput.* 219, 10853–65.

Rocha, H., J., D., Ferreira, B., Lopes, M., 2013c. Selection of intensity modulated radiation therapy treatment beam directions using radial basis functions within a pattern search methods framework. *J. Glob. Optim.* 57, 1065–89.

Rocha, H., J., D., Ventura, T., Ferreira, B., Lopes, M., 2016. A derivative-free multistart framework for an automated noncoplanar beam angle optimization in imrt. *Med. Phys.* 43, 5514–5526.

Rocha, H., J., D., Ventura, T., Ferreira, B., Lopes, M., 2017. A global score-driven beam angle optimization in imrt. In *17th International Conference on Computational Science and Its Applications*, LNCS, Springer, pp. 77–90.

Stein, J., Mohan, R., Wang, X., Bortfeld, T., Wu, Q., Preiser, K., Ling, C., Schlegel, W., 1997. Number and orientation of beams in intensity-modulated radiation treatments. *Med. Phys.* 24, 149–160.

Ventura, T., Lopes, M.C., Ferreira, B., Khouri, L., 2016. Spiderplan: A tool to support decision-making in radiation therapy treatment plan assessment. *Rep. Pract. Oncol. Radiother.* 21, 508–516.

Voglis, C., Lagaris, I., 2009. Towards"ideal multistart". a stochastic approach for locating the minima of a continuous function inside a bounded domain. *App. Math. Comput.* 213, 1404–1415.